Preprints of the 21st IFAC World Congress (Virtual)
Berlin, Germany, July 12-17, 2020

Dynamical Modeling and Gait Optimization of a 2-D Modular Snake Robot in a Confined Space

K.H.J. Classens [*,****] **M.A.J. Koopaee** [**] **C. Pretty** [**]
S. Weiland [*] **X. Chen** [***]

[*] *Department of Electrical Engineering, Eindhoven University of Technology, Eindhoven, The Netherlands*
[**] *Department of Mechanical Engineering, University of Canterbury, Christchurch, New Zealand*
[***] *Manufacturing Futures Research Institute, Swinburne University of Technology, Melbourne, Australia*
[****] *(e-mail: k.h.j.classens@tue.nl)*

Abstract: A model-based optimal gait is obtained for the 2-D locomotion of a modular snake robot in a duct. Optimality is considered in the sense of traveling as fast as possible or traveling with minimal energy consumption. The novelty of the work lies in the development of a framework to cast the full dynamic behavior, including contact constraints with simple objects, into an optimization problem which allows for gait parameter, control parameter and/or physical parameter optimization. Optimal gait and control parameters are found via a surrogate optimization procedure which reveals optimal locomotion strategies depending on the duct width and optimization criteria. The framework is tested and illustrated with a number of optimizations of 2-D locomotion of a snake robot where either traveling time or energy consumption is minimized.

Keywords: Dynamic modeling, Snake robot, Model-Based control, Global optimization

1. INTRODUCTION

Learning from natural phenomena has been an inspiration for engineers for decades. A fascinating field of research includes biologically inspired robotics under which the movement pattern of a snake robot may be categorized. The inherent hyper redundancy of snake robots makes them difficult to control, but results in enhanced mobility with respect to conventional robots. Due to their small cross-section, snake robots are ideal for locomotion in confined spaces such as ducts. For several years, research has been conducted on snake robots. The first reported analytical studies are from Gray (1946). Several decades later, Hirose (1946) built the first actual snake robot. In the last decades, multiple modeling approaches have been shown, as well as novel developments in snake robot mechanisms and their control Liljebäck et al. (2013). The term 'obstacle-aided locomotion', implying to propel via contact with the environment, has been introduced by means of a hybrid model in Transeth et al. (2008); Liljeback et al. (2009). Purely based on kinematics, simulation of the locomotion in a pipe and its experimental validation have been shown in Trebuňa et al. (2015, 2016); Virgala et al. (2018). The work of Rollinson and Choset (2016) demonstrates the use of snake robots in pipe networks. In Enner et al. (2013), an estimation method for pipe crawling and pole climbing is shown supported by experimental results.

This paper contributes in casting the 2-D locomotion problem of a modular snake robot as a single optimization problem in which gait parameters, control parameters and physical parameters are simultaneously optimized. Here optimal behavior will either mean travelling as far as possible or with minimal energy consumption to traverse a distance in a confined space. Control strategies for either of these optimizations are proposed. This paper will focus on a 2-D confined space, but extensions to 3-D are possible.

This paper is organised as follows. Section 2 discusses the kinematics. The optimization problem is formulated in Section 3 for different control objectives. The motion dynamics and the contact model with surface friction as well as the contact with the duct walls are derived in Sections 4 and 5, respectively. The simulation parameters and optimization strategies are defined in Section 6. Optimal gait trajectories and the influence of control parameters will be examined for either of the cases where the aim amounts to traveling as fast as possible or where the aim amounts to minimizing energy consumption.

2. KINEMATICS

We consider a modular snake robot that consists of n links as depicted in the schematic drawing shown in Fig. 1. It is assumed that all linked elements have the same mass m and inertia J. For simplicity, we assume that a link is symmetric with length $2l$, meaning that its center of mass is located at a distance l from either end. The vector in the global $(\boldsymbol{x}, \boldsymbol{y})$-plane indicating the location of the center of mass of link $i \in \{1, \ldots, n\}$ is given by

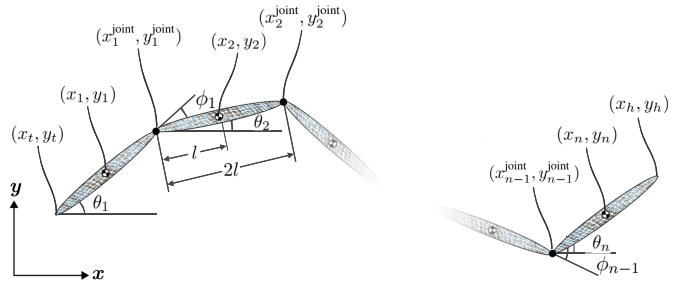

Fig. 1. Schematic snake robot in the $(\boldsymbol{x}, \boldsymbol{y})$-plane with n links.

$r_i = [x_i, y_i]^\top$. The vector pointing to the tail of the snake robot is defined by $r_t = [x_t, y_t]^\top$. The center of mass of the snake robot is indicated by $r_p = [p_x, p_y]^\top$. The absolute angle and the torque applied to of each link are denoted by θ_i and τ_i, respectively. The relative angle between the links is $\phi_i = \theta_i - \theta_{i+1}$, where $i \in \{1, \ldots, n-1\}$. To write the kinematics of the snake robot in matrix form, some vectors and matrices will be defined as follows. The vectors of absolute and relative angles are defined as $\theta := [\theta_1, \ldots, \theta_n]^\top$ and $\phi := [\phi_1, \ldots, \phi_{n-1}]^\top$, respectively. Let $\tau := [\tau_1, \ldots, \tau_{n-1}]^\top$ be the vector of all torques. Trigonometric functions of vectors are defined entry-wise as in $\sin(\theta) := [\sin(\theta_1), \ldots, \sin(\theta_n)]^\top$. Restructuring these into $n \times n$ diagonal matrices gives $S_\theta := \operatorname{diag}(\sin(\theta))$ and $C_\theta := \operatorname{diag}(\cos(\theta))$. The coordinates of all links are stacked in $x := [x_1, \ldots, x_n]^\top$ and $y := [y_1, \ldots, y_n]^\top$. To represent these coordinates as a function of θ and the tail coordinates r_t, we define the $n \times n$ matrix G where $G_{ij} = l$ if $i = j$, $G_{ij} = 2l$ if $i > j$ and $G_{ij} = 0$ if $i < j$. The coordinates of the links in the global reference frame can then be written as

$$x = ex_t + G\cos(\theta) \tag{1a}$$

and

$$y = ey_t + G\sin(\theta), \tag{1b}$$

where $e = [1, \ldots, 1]^\top$ is a vector of length n. Similarly, their velocities are expressed as

$$\dot{x} = e\dot{x}_t - GS_\theta\dot{\theta} \tag{2a}$$

and

$$\dot{y} = e\dot{y}_t + GC_\theta\dot{\theta}. \tag{2b}$$

The coordinates of the center of mass of the robot can be inferred from $r_p = [p_x, p_y]^\top = \frac{1}{n}[e^\top x, e^\top y]^\top$. Similarly, its velocity $\dot{r}_p = \frac{1}{n}[e^\top \dot{x}, e^\top \dot{y}]^\top$. For the tail coordinates of the robot we can rewrite these expressions as

$$x_t = p_x - \frac{1}{n}e^\top G\cos(\theta) \tag{3a}$$

and

$$y_t = p_y - \frac{1}{n}e^\top G\sin(\theta). \tag{3b}$$

The linear velocity of the tail of the robot then satisfies

$$\dot{x}_t = \dot{p}_x + \frac{1}{n}e^\top GS_\theta\dot{\theta} \tag{4a}$$

and

$$\dot{y}_t = \dot{p}_y - \frac{1}{n}e^\top GC_\theta\dot{\theta}. \tag{4b}$$

3. PROBLEM FORMULATION

It is desired to control the body shape of the snake robot so as to optimize its locomotion in a well defined sense and without any prior knowledge regarding the way the robot interacts with its environment. In this paper, we restrict ourselves to two relevant optimization criteria. The first objective amounts to maximizing the traveled distance in an *a priori* specified time window. We focus here on 1-D movements in the x-direction, which means that this objective is interpreted as maximizing the traveled distance of the center of mass p_x of the entire snake robot in a given time window $T > 0$. Hence, the objective is to

$$\begin{aligned} &\underset{z}{\text{maximize}} \; p_x(z, t = T) \\ &\text{subject to } h(z) \leq 0, \end{aligned} \tag{5}$$

where $z \in \mathcal{Z} \subseteq \mathbb{R}^{n_z}$ denotes a vector representing all design variables and h is a vector-valued function representing all inequality constraints incurred by the model and design constraints to be defined below.

The second objective amounts to minimizing energy consumption during locomotion. Since autonomous snake robots are usually operated by battery cells with limited energy capacity, it is of evident interest to minimize energy consumption. This objective is formalized by maximizing the traveled distance per unit of consumed energy as

$$\begin{aligned} &\underset{z}{\text{maximize}} \; \frac{p_x(z, t = T)}{\int_0^T \left|\dot{\phi}^\top \tau\right| \mathrm{d}t} \\ &\text{subject to } h(z) \leq 0 \end{aligned} \tag{6}$$

where the denominator of the cost function represents the total supplied energy to the robot in the time interval $[0, T]$.

4. DYNAMICS

The equations of motion for the modular snake robot are derived using Lagrangian mechanics by setting

$$\left(\frac{\mathrm{d}}{\mathrm{d}t}\left(\frac{\partial T}{\partial \dot{q}}\right) - \frac{\partial T}{\partial q} + \frac{\partial V}{\partial q}\right)^\top = Q, \tag{7}$$

where T equals the kinetic energy, V is the potential energy and Q contains the non-conservative generalized forces and moments. Here, q denotes the position vector of generalized coordinates

$$q := [\phi_1, \ldots, \phi_{n-1}, \theta_n, p_x, p_y]^\top. \tag{8}$$

Thus, the first $n-1$ variables denote the relative angles among the links. The remaining three coordinates are the absolute angle of the head θ_n and the coordinates of the center of mass. Since $\theta_i = \sum_{m=i}^{n-1} \phi_m + \theta_n$, the vector of absolute angles θ can be written as

$$\theta = \underbrace{[H \;\; e \;\; 0_{n\times 2}]}_{C} q, \tag{9}$$

where the $n \times (n-1)$ matrix $H_{ij} = 1$ if $i \leq j$ and $H_{ij} = 0$ if $i > j$. With the latter, (1) can be rewritten as function of the generalized coordinates as

$$x = \underbrace{[0_{n\times n} \;\; e \;\; 0_{n\times 1}]}_{B_x} q - \underbrace{\left(-G + \frac{1}{n}ee^\top G\right)}_{A} \cos(Cq) \tag{10a}$$

and

$$y = \underbrace{[0_{n\times n}\ 0_{n\times 1}\ e]}_{B_y} q - \underbrace{\left(-G + \frac{1}{n} e e^\top G\right)}_{A} \sin(Cq), \quad (10b)$$

where the matrices A, B_x, B_y, and C are real valued. In a similar fashion, (2) can be rewritten as

$$\dot{x} = B_x \dot{q} + A S_\theta C \dot{q} \quad (11a)$$

and

$$\dot{y} = B_y \dot{q} - A C_\theta C \dot{q}. \quad (11b)$$

The total kinetic energy is the sum of the translational energy and the rotational energy of each link. This means that the kinetic energy

$$T(q, \dot{q}) = \frac{1}{2} m \dot{x}^\top \dot{x} + \frac{1}{2} m \dot{y}^\top \dot{y} + \frac{1}{2} J \dot{\theta}^\top \dot{\theta}. \quad (12)$$

In the case of planar locomotion, there is no component that contributes to the potential energy, hence we set $V = 0$. Now that expressions are determined for T and V, the left hand side of (7) is established. Explicit expressions for the derivatives with respect to q and $\dot{q}$ are described in Koopaee et al. (2019). The sum of all non-conservative generalized forces and moments acting on the robot define the right hand side of (7) and can be written as

$$Q = \sum_{j=1}^{n_F} \left(\frac{\partial r_j}{\partial q}\right)^\top F_j + \sum_{k=1}^{n_M} \left(\frac{\partial \Theta_k}{\partial q}\right)^\top M_k. \quad (13)$$

Here, n_F and n_M denote the number of non-conservative forces and non-conservative moments, respectively. The generalized non-conservative force vector j is denoted by F_j and the generalized non-conservative moment k is denoted by M_k. The absolute position vector of the j^{th} force is denoted by r_j and the absolute rotation vector of the k^{th} moment is denoted by Θ_k. The non-conservative generalized force vector is split in three components as

$$Q = Q^{\text{act}} + Q^{\text{sur}} + Q^{\text{env}}, \quad (14)$$

where Q^{act} represents the actuator torques, Q^{sur} represents the frictional surface forces and Q^{env} contains the forces exerted by the environment. The distribution of the applied torques over the various joints is encoded in matrix D so that

$$Q^{\text{act}} = D\tau, \quad (15)$$

where $D = \begin{bmatrix} I_{(n-1)} & 0_{(n-1)\times 3} \end{bmatrix}^\top$ in which $I_{(n-1)}$ is an identity matrix of size $n-1$ and $0_{(n-1)\times 3}$ is a zero matrix of size $(n-1)\times 3$.

5. CONTACT MODEL

This section is devoted to discussing surface friction and forces exerted by the environment. It is shown how to incorporate these in Q^{sur} and Q^{env}.

5.1 Surface Friction

If the snake is moving in the horizontal plane, there is a certain surface friction. This surface friction is incorporated in the model by applying the frictional force at the center of mass of each link as depicted in Fig. 2. A Coulomb type of friction, acting on link i, is incorporated as

$$\begin{bmatrix} F^{\text{Cou}}_{\text{tan},i} \\ F^{\text{Cou}}_{\text{nor},i} \end{bmatrix} = -mg \begin{bmatrix} \mu_{\text{tan}} & 0 \\ 0 & \mu_{\text{nor}} \end{bmatrix} \text{sign}\left(\begin{bmatrix} v_{\text{tan},i} \\ v_{\text{nor},i} \end{bmatrix}\right), \quad (16)$$

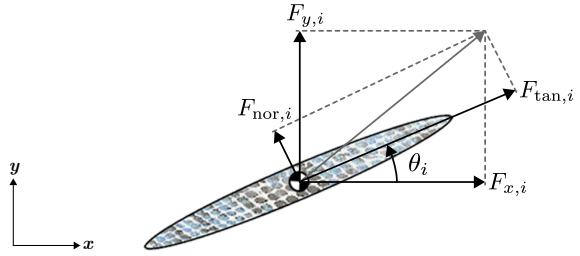

Fig. 2. Rotation from the local link coordinate system to the global coordinate system.

where g is the gravitational constant and μ_{tan} and μ_{nor} denote the friction coefficient in tangential and normal direction, respectively. The tangential and normal velocity of link i are written as $v_{\text{tan},i}$ and $v_{\text{nor},i}$. Similarly, a viscous component is added as

$$\begin{bmatrix} F^{\text{vis}}_{\text{tan},i} \\ F^{\text{vis}}_{\text{nor},i} \end{bmatrix} = - \begin{bmatrix} \nu_{\text{tan}} & 0 \\ 0 & \nu_{\text{nor}} \end{bmatrix} \begin{bmatrix} v_{\text{tan},i} \\ v_{\text{nor},i} \end{bmatrix}, \quad (17)$$

where ν_{tan} and ν_{nor} are the viscous friction coefficients. Note that the frictional forces are always acting in opposite direction with respect to the local direction of motion. To transform the local forces to the global coordinate frame, a coordinate transformation is applied via a rotation matrix R. In the global coordinate frame, the frictional forces are obtained from a counter-clockwise rotation matrix

$$R_i := \begin{bmatrix} \cos(\theta_i) & -\sin(\theta_i) \\ \sin(\theta_i) & \cos(\theta_i) \end{bmatrix}$$

by setting

$$\begin{bmatrix} F_{x,i} \\ F_{y,i} \end{bmatrix} = R_i \begin{bmatrix} F_{\text{tan},i} \\ F_{\text{nor},i} \end{bmatrix}. \quad (18)$$

Here, $F_{\text{tan},i} = F^{\text{Cou}}_{\text{tan},i} + F^{\text{vis}}_{\text{tan},i}$ and $F_{\text{nor},i} = F^{\text{Cou}}_{\text{nor},i} + F^{\text{vis}}_{\text{nor},i}$. To incorporate these forces in (13) (and hence in (7)), the forces in x and y-direction will be stacked as $F_x := [F_{x,1}, \ldots, F_{x,n}]^\top$ and $F_y := [F_{y,1}, \ldots, F_{y,n}]^\top$. The surface friction is then defined as

$$Q^{\text{sur}} = \begin{bmatrix} (B_x + A S_\theta C)^\top & (B_y - A C_\theta C)^\top \end{bmatrix} \begin{bmatrix} F_x \\ F_y \end{bmatrix}. \quad (19)$$

5.2 Environment Model

A snake robot is able to exploit contact with the environment to its advantage. An example of this is where the snake robot is in contact with a wall when moving in a duct. In the model of the snake robot, we assume that the head, the tail and the joints are allowed to exchange forces via contact with the environment. To model this, it is necessary to identify the coordinates that make direct contact. Similar expressions to (10) and (11) can be derived. For any coordinate that makes contact with an environmental constraint, a penalizing normal force will be exerted at this position coordinate according to

$$F_{\text{nor}} = \begin{cases} \max(kw - dv_{\text{nor}}, 0) & \text{if} \quad w > 0 \\ 0 & \text{if} \quad w \leq 0, \end{cases} \quad (20)$$

where w is the distance that the head, tail or joint exceeds the environmental boundary and where v_{nor} denotes the local normal velocity, directed perpendicular to the boundary. The max operator is used to prevent the environment pulling on the robot. Only a normal force is desired. The parameters k and d are positive real numbers that

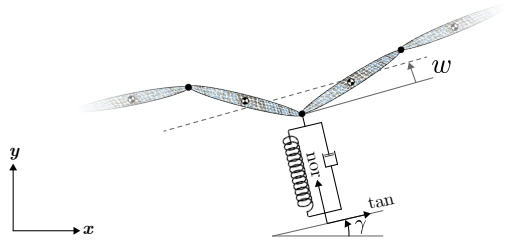

Fig. 3. Environmental model represented as a spring-damper system.

represent the elasticity and damping of the environment. Notice that one can interpret this force as a spring-damper system that becomes active only when the robot makes contact with the boundary and where only a positive force can be exerted. This is schematically represented in Fig. 3. Similar to the modeling of the surface friction, there is also a tangential force at contact locations which is modeled as

$$F_{\tan} = -F_{\mathrm{nor}}\mu_o \mathrm{sign}\left(v_{\tan}\right) - \nu_o v_{\tan}, \tag{21}$$

where μ_o and ν_o are the Coulomb and viscous friction coefficients of the wall. Here, $v_{\tan}$ is the local tangential velocity. In case of a duct, suppose that its wall is oriented at an angle γ. In the global reference frame, the normal and tangential force are represented by

$$\begin{bmatrix} F_x \\ F_y \end{bmatrix} = R_\gamma \begin{bmatrix} F_{\tan} \\ F_{\mathrm{nor}} \end{bmatrix}, \tag{22}$$

where

$$R_\gamma := \begin{bmatrix} \cos\left(\gamma\right) & -\sin\left(\gamma\right) \\ \sin\left(\gamma\right) & \cos\left(\gamma\right) \end{bmatrix}.$$

The force vectors $\bar{F}_x := [F_{x,t}, F_{x,1}^{\mathrm{joint}}, \ldots, F_{x,n-1}^{\mathrm{joint}}, F_{x,h}]^\top$ and $\bar{F}_y := [F_{y,t}, F_{y,1}^{\mathrm{joint}}, \ldots, F_{y,n-1}^{\mathrm{joint}}, F_{y,h}]^\top$. The environmental forces are then incorporated in Q^{env} as

$$Q^{\mathrm{env}} = \begin{bmatrix} \left(\bar{B}_x + \bar{A}S_\theta C\right)^\top & \left(\bar{B}_y - \bar{A}C_\theta C\right)^\top \end{bmatrix} \begin{bmatrix} \bar{F}_x \\ \bar{F}_y \end{bmatrix}. \tag{23}$$

This completes the specific modeling of all terms in (14).

6. CONTROL STRATEGY AND OPTIMIZATION

The torque vector τ is used to control the movements and body shape of the snake robot. The equations of motion, obtained from (7), are structured such that the actuated dynamics are separated from the unactuated dynamics as

$$\underbrace{\begin{bmatrix} M_{11} & M_{12} \\ M_{21} & M_{22} \end{bmatrix}}_{M(q)} \begin{bmatrix} \ddot{q}_a \\ \ddot{q}_u \end{bmatrix} + \underbrace{\begin{bmatrix} N_1 \\ N_2 \end{bmatrix}}_{N(q,\dot{q})} = \underbrace{\begin{bmatrix} \tau \\ 0_{3\times 1} \end{bmatrix}}_{D\tau} + \begin{bmatrix} Q_1^{\mathrm{sur}} \\ Q_2^{\mathrm{sur}} \end{bmatrix} + \begin{bmatrix} Q_1^{\mathrm{env}} \\ Q_2^{\mathrm{env}} \end{bmatrix}, \tag{24}$$

where $M(q)$ is the inertia matrix and $N(q,\dot{q})$ accounts for the centrifugal and Coriolis terms. The generalized coordinates are partitioned into an actuated part, $q_a := [\phi_1, \ldots, \phi_{n-1}]^\top$, and an unactuated part $q_u := [\theta_n, p_x, p_y]^\top$. Due to the structure of D, the actuated dynamics are directly controlled by the joint torques τ_i. The unactuated coordinates represent position and orientation of the snake robot in the global coordinate system.

An arbitrary 2-D duct is modeled by two walls at heights $y = y_{\min}$ and $y = y_{\max}$ with orientations defined by angles $\gamma_{\min} = 0^\circ$ and $\gamma_{\max} = 180^\circ$, resp. (enabling a proper orientation of the exerted forces). In this study, a snake robot consisting of $n = 10$ links will be considered. Each link is considered to be a slender rod and has an inertia of $J = 1/12ml^2$ around its center of mass. The other parameters are given in Table 1. Note that a relatively high stiffness k is required since the walls are assumed to be close to rigid. The surface friction parameters are chosen to be equal in tangential and normal direction such that the robot has to use the environment in order to propel.

Table 1. Simulation Parameters

Parameter	Unit	Value	Parameter	Unit	Value
l	m	0.1	k	N/m	500
m	kg	0.1	d	Ns/m	25
μ_t, μ_n	-	1	μ_0	-	1
ν_t, ν_n	Ns/m	1	ν_0	Ns/m	1

The torque control vector τ is determined on the basis of a partial feedback linearized input as in Spong (1994), where the transformation

$$\tau = \left(M_{11} - M_{12}M_{22}^{-1}M_{21}\right)\bar{\tau} + N_1 - Q_1^{\mathrm{sur}} - M_{12}M_{22}^{-1}\left(N_2 - Q_2^{\mathrm{sur}}\right) \tag{25}$$

results in the dynamics

$$\begin{aligned} \ddot{q}_a &= \bar{\tau} + \left(M_{11} - M_{12}M_{22}^{-1}M_{21}\right)^{-1}\left(Q_1^{\mathrm{env}} - M_{12}M_{22}^{-1}Q_2^{\mathrm{env}}\right) \\ \ddot{q}_u &= f\left(M\left(q\right), N\left(q\right), Q^{\mathrm{sur}}, Q^{\mathrm{env}}, \bar{\tau}\right), \end{aligned} \tag{26}$$

in which $\bar{\tau}$ is the new control input and f represents the (non-linear) vector field of the unactuated dynamics. Hence, the influence of contact with environmental constraints is not linearized in this model because these influences are assumed unknown or unmeasurable.

The applied torque input in joint i is assumed to be of the standard proportional-derivative control form

$$\bar{\tau}_i = \ddot{\phi}_i^{\mathrm{ref}} + k_d\left(\dot{\phi}_i^{\mathrm{ref}} - \dot{\phi}_i\right) + k_p\left(\phi_i^{\mathrm{ref}} - \phi_i\right) \tag{27}$$

with control parameters k_d and k_p independent of i. For $k_d > 0$ and $k_p > 0$ the undisturbed system (without contact with the environment), gives exponentially stable joint dynamics, as shown in Liljebäck et al. (2013); Khalil (2002), since without contact $\ddot{q}_a = \bar{\tau}$. The reference signal that will be used will be confined to signals of the type

$$\phi_i^{\mathrm{ref}}(t) = a\sin\left(\omega t - (i-1)\delta\right), \tag{28}$$

where a denotes the amplitude of the joint angle, ω is the angular frequency and δ is the phase shift among the joints. That is, we aim to track a sinusoidal reference signal at frequency ω, amplitude a and a joint-dependent phase. With the described dynamical model, the control strategy and the body shape reference, one can simulate the locomotion in a duct.

Apart from the inequality constraints on the controller parameters, we also add two termination criteria to the simulation. We do not want the snake to push too hard against the wall. In such case, the simulation will be terminated prematurely and the objective function (5) or (6) will return zero. This termination occurs when the amplitude $\|\bar{F}_y(t)\|_\infty > F_{\max}$. Similarly, a simulation will be terminated if $\|\theta(t)\|_\infty > \theta_{\max}$. The latter criterion is used to prevent the possibility of links to get jammed. Throughout this study, we set $F_{\max} = 25$ N and $\theta_{\max} = \pi$. The time window is taken by setting $T = 20$ s.

The evaluation of the cost functions (5) and (6) requires a dynamical model simulation over a time window of length T. With $n = 10$ and $T = 20$ s this simulation takes around 10 seconds and is computationally expensive. Therefore,

a surrogate optimization routine is used to find the optimum. This surrogate optimization routine is proven to converge to a global solution in Gutmann (2001) and is a feasible trade-off between the speed of the algorithm and the exploration in the design parameter space. The surrogate optimization is constructed by interpolating cubic radial basis functions with a linear tail through objective function evaluations.

6.1 Optimization in (a, δ)-space

First, both optimizations (5) and (6) will be performed, where the design variables are stacked in $z := [a, \delta]^\top \in \mathcal{Z}$, where $\mathcal{Z} := ([0, 3] \times [0, \pi])$. These bounds on the gait parameters are incorporated in the constraint function $h(z)$. For now, the angular frequency is kept constant at $\omega = 2/5\pi$ rad. That is, the controller (27) is assumed to be fixed with $k_p = 100$ and $k_d = 25$. A $T = 20$ s simulation will be performed for each pair (a, δ). First, a wide duct is used with $y_{\min} = -0.125$ m and $y_{\max} = 0.125$ m. The objective function evaluations are shown in Fig. 4 and Fig. 5 for both objective functions. The optimal solution (a^*, δ^*) solving (5) is $(1.986, 1.456)$ rad and is used to simulate the trajectory of the robot snake over time. Snapshots of this simulation are depicted in Fig. 6. Similarly, snapshots of the optimal solution solving (6) are shown. In this case, the optimal solution $(a^*, \delta^*) = (1.022, 1.238)$ rad. One can conclude that the body shape to propel as fast as possible resembles a transverse wave. This type of body shape pushes its joints against the wall. This force induces a significant error in terms of joint angle, hence resulting in significant control energy. The energy efficient behavior is similar, but makes little contact with the wall which is just enough in order to propel, therefore requiring less control effort.

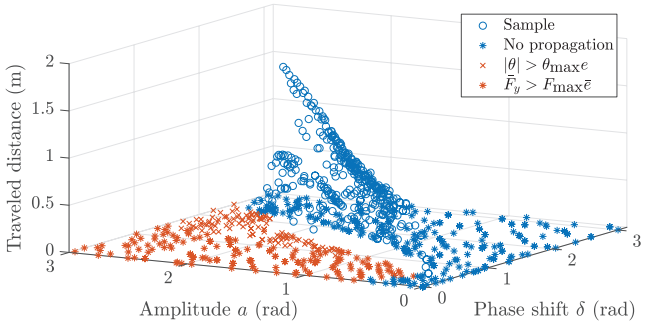

Fig. 4. Distance objective function for a wide duct.

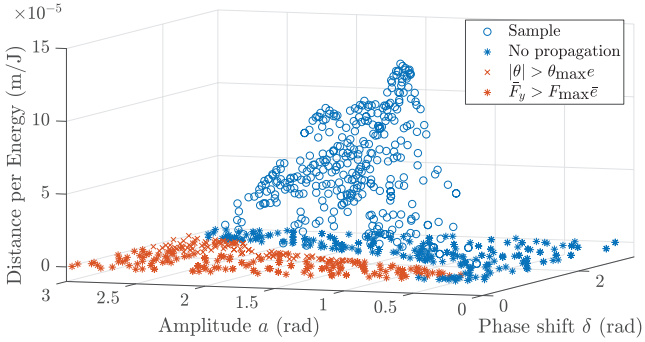

Fig. 5. Energy objective function for a wide duct.

A similar gait optimization is performed in a narrower duct, where $y_{\min} = -0.075$ m and $y_{\max} = 0.075$ m. In this case, the optimal solutions (a^*, δ^*) of (5) and (6) are given by $(2.625, 2.944)$ rad and $(1.891, 2.712)$ rad respectively. The locomotion, using the optimal solutions are shown in Figure 7. The optimal gait is significantly different in this narrow duct. It can be concluded that the robot propels faster. The robot clamps itself down on the tail end by pushing against the wall, after which it extends. Subsequently, the robot clamps its head down and and retracts, showing resemblance to a longitudinal wave.

6.2 Optimization in (k_p, k_d)-space

To investigate the influence of the control gains another optimization will be performed. Now, the gait parameters are fixed to $a = 1$ rad, $\delta = 1$ rad and $\omega = 2/5\pi$ rad. Note that this will yield a body shape reference in the form of a traveling wave, close to what is shown in Fig. 6. We will optimize the criteria (5) and (6) over the controller gains $[k_p, k_d]^\top =: z$ that are assumed to reside in $\mathcal{Z} := ([0, 1000] \times [0, 1000])$. We will confine ourselves to the case of the wide duct where $y_{\min} = -0.125$ m and $y_{\max} = 0.125$ m. The objective function evaluations are

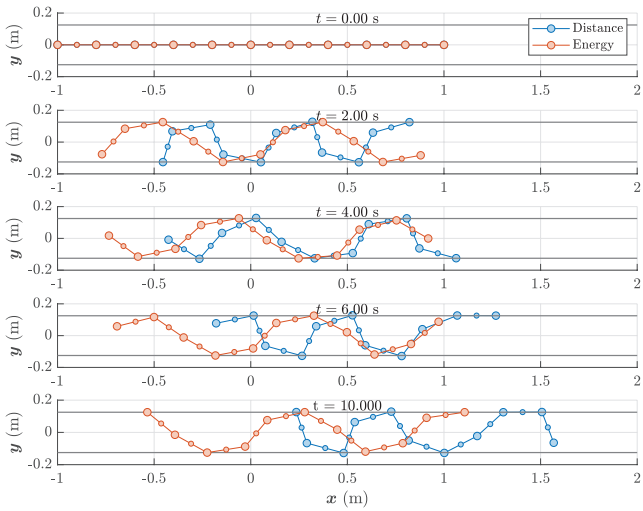

Fig. 6. Snapshots of a robot with 10 links in a wide duct.

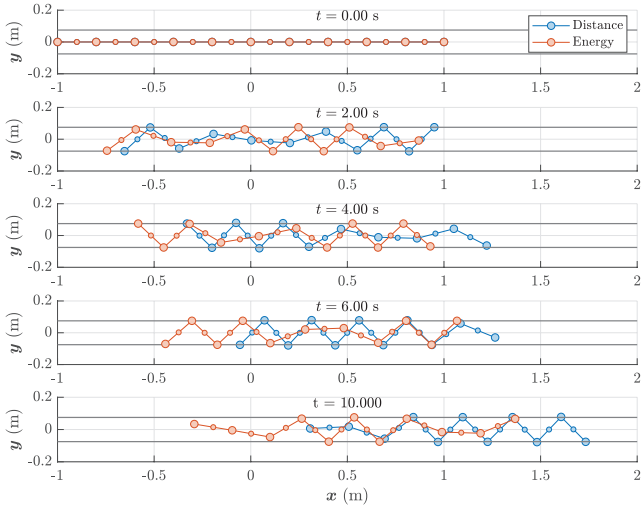

Fig. 7. Snapshots of a robot with 10 links in a narrow duct.

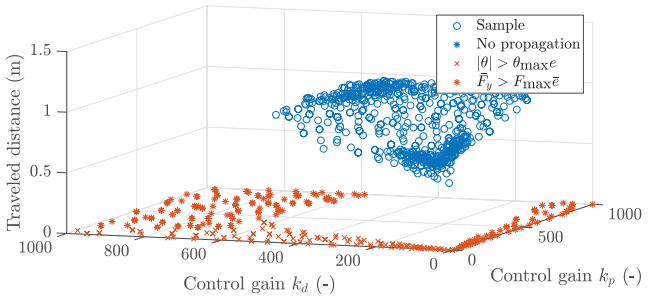

Fig. 8. Distance objective function for varying control gains.

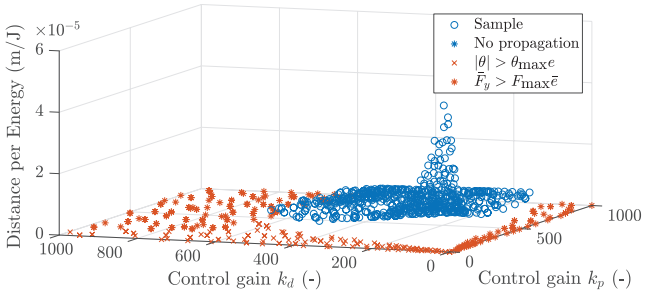

Fig. 9. Energy objective function for varying control gains.

shown in Fig. 8 and Fig. 9. It can be concluded, that a high value of k_d will yield a solution that pushes too hard against the wall. Regarding the achieved distance, the influence of k_p and k_d is limited as long as there is contact with the wall. However, in terms of energy efficiency, a low control gain will perform significantly better.

6.3 Optimization in $(a, \delta, \omega, k_d, k_p)$-space

Finally, we will examine the influence of all aforementioned decision variables in the optimization problems (5) and (6). The decision variables are taken as $z := [a, \delta, \omega, k_p, k_d]^\top \in \mathcal{Z}$, where $\mathcal{Z} := ([0, 3] \times [0, \pi] \times [0, 2\pi] \times [0, 1000] \times [0, 1000])$. Again, we will confine ourselves to the case of the wide duct where $y_{\min} = -0.125$ m and $y_{\max} = 0.125$ m. The optimal solutions $(a^*, \delta^*, \omega^*, k_p^*, k_d^*)$ of (5) and (6) are given by $(1.426 \text{ rad}, 1.319 \text{ rad}, 6.162 \text{ rad}, 935.321, 280.313)$ and $(1.237 \text{ rad}, 0.940 \text{ rad}, 0.171 \text{ rad}, 330.079, 391.064)$ respectively. Both criteria show that there is a corresponding optimal combination of amplitude a and phase shift δ. To maximize traveled distance, a high ω and k_p is desired. To be energy efficient, a low ω is desired to have less viscous friction and to reduce the control error.

7. CONCLUSION AND FUTURE WORK

In this paper, a modeling framework is presented to optimize the 2-D locomotion of a modular snake robot where the spring-damper contact model enables to model different environments such as a duct. The surrogate optimization routine shows how the model could be used for optimization based on a velocity or energy efficiency criterion. It shows that for locomotion in a duct, optimal gaits are significantly different depending on the duct width and the objective. An energy effient locomotion requires a low angular frequency and low control gains. A fast locomotion is obtained with a high angular frequency and higher control gains. The modeling strategy that is developed here is generic and scalable and can be easily extended to include gravitational effects. Although we have considered locomotion in ducts in the paper, the environmental model is completely flexible and independent from the kinematics. Also physical parameters such as the link length may be optimized for a specific task. In Koopaee et al. (2019), rectilinear locomotion over an obstacle will be demonstrated using an adaptive control strategy. In Koopaee et al. (2020), the model will be extended to incorporate the influence of series elastic actuators. Its effect on the locomotion over obstacles will be discussed and is supported by experimental validation.

REFERENCES

Enner, F., Rollinson, D., and Choset, H. (2013). Motion estimation of snake robots in straight pipes. In *2013 IEEE International Conference on Robotics and Automation*, 5168–5173. IEEE, Karlsruhe, Germany. doi:10.1109/ICRA.2013.6631316.

Gray, J. (1946). The Mechanism of Locomotion in Snakes. *Journal of Experimental Biology*, 23(2).

Gutmann, H. (2001). A Radial Basis Function Method for Global Optimization. *Journal of Global Optimization*. doi: 10.1023/A:1011255519438.

Hirose, S. (1946). *Biologically Inspired Robots: Snake-like Locomotors and Manipulators*. Oxford University Press.

Khalil, H.K. (2002). *Nonlinear Systems*. Pearson, Upper Saddle River, N.J, 3 edition edition.

Koopaee, M.J., Pretty, C., Classens, K.H.J., and Chen, X. (2019). Dynamical Modelling and Control of Snake-Like Motion in Vertical Plane for Locomotion in Unstructured Environments. In *15th IEEE/ASME International Conference on Mechatronic and Embedded Systems and Applications*. American Society of Mechanical Engineers, Anaheim, California, USA. doi:10.1115/DETC2019-97227.

Koopaee, M.J., Pretty, C., Classens, K.H.J., and Chen, X. (2020). Dynamical Modeling and Control of Modular Snake Robots With Series Elastic Actuators for Pedal Wave Locomotion on Uneven Terrain. *Journal of Mechanical Design*, 142(3). doi: 10.1115/1.4044691.

Liljeback, P., Pettersen, K., and Stavdahl, O. (2009). Modelling and control of obstacle-aided snake robot locomotion based on jam resolution. In *2009 IEEE International Conference on Robotics and Automation*, 3807–3814. IEEE, Kobe. doi: 10.1109/ROBOT.2009.5152273.

Liljebäck, P., Pettersen, K.Y., Stavdahl, O., and Gravdahl, J.T. (2013). *Snake Robots: Modelling, Mechatronics, and Control*. Advances in Industrial Control. Springer-Verlag, London.

Rollinson, D. and Choset, H. (2016). Pipe Network Locomotion with a Snake Robot: Pipe Network Locomotion with a Snake Robot. *Journal of Field Robotics*, 33(3), 322–336. doi:10.1002/rob.21549.

Spong, M. (1994). Partial feedback linearization of underactuated mechanical systems. In *Proceedings of IEEE/RSJ International Conference on Intelligent Robots and Systems*. doi: 10.1109/IROS.1994.407375.

Transeth, A., Leine, R., Glocker, C., Pettersen, K., and Liljeback, P. (2008). Snake Robot Obstacle-Aided Locomotion: Modeling, Simulations, and Experiments. *IEEE Transactions on Robotics*, 24(1), 88–104. doi:10.1109/TRO.2007.914849.

Trebuňa, F., Virgala, I., Kelemen, M., and Lipták, T. (2015). Locomotion of Snake Robot through the Pipe. *Journal of Automation and Control*, 3(3), 135–139. doi:10.12691/automation-3-3-20.

Trebuňa, F., Virgala, I., Pástor, M., Lipták, T., and Miková, Ľ. (2016). An inspection of pipe by snake robot. *International Journal of Advanced Robotic Systems*, 13(5). doi: 10.1177/1729881416663668.

Virgala, I., Lipták, T., and Miková, Ľ. (2018). Snake Robot Locomotion Patterns for Straight and Curved Pipe. *Journal of Mechanical Engineering*, 68(2). doi:10.2478/scjme-2018-0020.